Eigenmode excitation of Alfven ion cyclotron instability

doi: 10.1063/1.872067

Eigenmode excitation of Alfvén ion cyclotron instability

R. Katsumata,[a] M. Ichimura, M. Inutake,[b] H. Hojo, A. Mase, and T. Tamano
Plasma Research Center, University of Tsukuba, Ibaraki 305, Japan

(Received 22 February 1996; accepted 26 August 1996)

In the GAMMA 10 tandem mirror [M. Inutake *et al.*, Phys. Rev. Lett. **55**, 939 (1985)], plasmas with a high beta value (ratio of plasma pressure to magnetic pressure) are produced by using an ICRF (ion cyclotron range of frequency) heating. Magnetic field fluctuations identified as an Alfvén ion cyclotron (AIC) mode are excited with strong dependence on a perpendicular beta value and a temperature anisotropy $T_\perp/T_\parallel$ (a ratio between the temperatures perpendicular and parallel to the magnetic field line). Spatial structures and excitation conditions of the AIC mode are experimentally studied. AIC modes are spontaneously excited as axial eigenmodes, of which boundary is determined by the reflection point in anisotropic plasmas. The AIC mode in the GAMMA 10 is observed well below the theoretically predicted threshold. © *1996 American Institute of Physics.* [S1070-664X(96)00812-9]

I. INTRODUCTION

An Alfvén ion cyclotron mode (AIC) is one of the microinstabilities that are driven by an anisotropy of the ion distribution function. Theoretical studies of the AIC mode have been made by many researchers.[1–8] In comparison with the theoretical studies, experimental studies in a laboratory are less advanced because of difficulties in producing plasmas with strong anisotropy and in measuring high-frequency magnetic fluctuations in a hot plasma.[9–13] Deterioration of plasma confinement, particularly in mirror devices, is concerned because fluctuations associated with the AIC mode may induce a diffusion in the velocity space. That is, ions are scattered into a loss cone in a time scale shorter than a Coulomb collision time.[14,15] Thus, it is of a crucial importance to study AIC modes in a tandem mirror. The first experimental observation of the AIC modes was made in the end-cell plasmas of the TMX (Tandem Mirror Experiment) device,[11,16] which were produced by perpendicularly injected high-energy neutral beams, and degradation of the confinement was reported. Stabilization of the AIC mode was achieved in the TMX-U device by reducing anisotropy with an oblique injection of a neutral beam. The AIC mode was also observed in the ion cyclotron range of frequency (ICRF) heated central-cell plasma of the TARA tandem mirror.[17] The criterion between the absolute and convective instabilities is theoretically predicted and is approximately given by[6]

$$\beta_\perp\left(\frac{T_\perp}{T_\parallel}\right)^2 \geqslant 3.5. \tag{1}$$

Here, $\beta_\perp$ is a plasma beta value and $T_\perp$ and $T_\parallel$ are temperatures perpendicular and parallel to the magnetic field line, respectively. In the TARA experiments, it has been noted that the experimentally observed threshold is in agreement with the theoretical criterion. Recently, magnetic fluctuations due to the AIC mode have also been observed in an ICRF-heated central cell plasma of the GAMMA 10 tandem mirror. The stability threshold of the AIC mode experimentally observed in GAMMA 10[15] is given by

$$\beta_\perp\left(\frac{T_\perp}{T_\parallel}\right)^2 \geqslant 0.3. \tag{2}$$

As described in the previous paragraph, according to the conventional theory for infinite and uniform plasmas, a convective AIC mode is not expected to grow into an observable fluctuation level in a finite length in the region of $\beta_\perp(T_\perp/T_\parallel)^2<3.5$.

In order to understand the experimental situation in the GAMMA 10, fine structures of the AIC mode are obtained in radial, azimuthal, and axial directions. From the axial wave number measurements, it becomes clear that the AIC mode has both a standing wave region and a propagating region in the axial direction. The observed AIC mode has the form of an eigenmode with boundaries in the axial direction. The outline of this paper is as follows: The experimental setup is described in Sec. II. The identification and the spatial structures of the AIC mode are presented in Sec. III. Some discussions and a conclusion are given in Sec. IV and in Sec. V.

II. EXPERIMENTAL SETUP

The GAMMA 10 is an axisymmetrized tandem mirror with a thermal barrier.[18] The GAMMA 10 consists of five mirror cells, which are a central cell, minimum-*B* anchor cells, and plug/barrier cells at both ends. The length of the central cell between mirror throats is 5.8 m and the diameter of the stainless-steel vacuum vessel is 1 m. Magnetic field strength at the midplane of the central cell is 0.41 T and the mirror ratio is 5 in a standard mode of operations. A limiter with a diameter of 0.36 m is set near the midplane. The anchor cells are located adjacent to the central cell and consist of minimum-*B* mirror fields produced by baseball seam coils. The anchor cell is so named since it is the stabilizing anchor cell for the magnetohydrodynamically (MHD) unstable central-cell plasma. The magnetic field strength is 0.61 T in the midplane of the anchor cell and the mirror ratio is 3. The plug/barrier cells are located at both ends of the

[a]Present address: ULSI Research Laboratory, Toshiba Corporation, Kawasaki, Kanagawa 210, Japan.
[b]Present address: Faculty of Engineering, Tohoku University, Sendai, Miyagi 980, Japan.

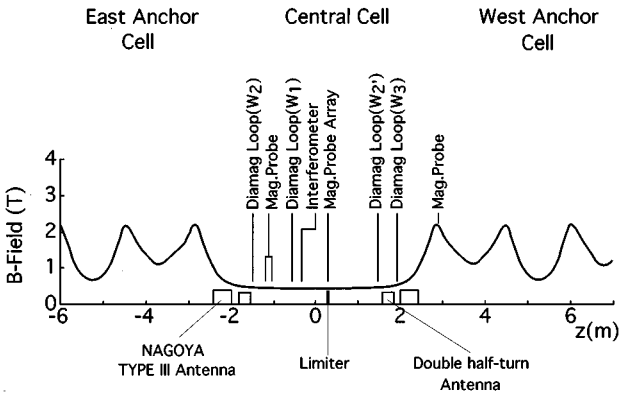

FIG. 1. The axial profile of magnetic field strength in the central and anchor cells of GAMMA 10. The locations of diagnostics are also shown.

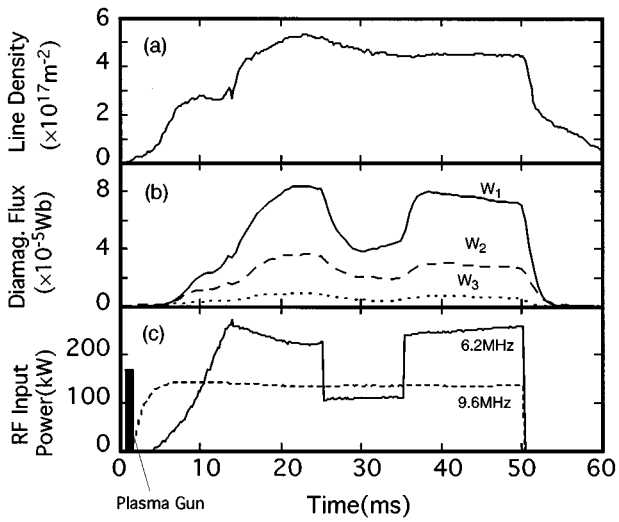

FIG. 2. Typical time evolutions of (a) an electron line density, (b) a diamagnetic loop signal in the central cell, and (c) supplied rf power of 6.2 and 9.6 MHz. The midplane loop signal is represented by W_1, the second loop signal W_2, and the third loop signal W_3. A supplied power to the double half-turn antenna for ion heating (6.2 MHz) in central cell is modulated down from 25 through 35 ms.

GAMMA 10, where a thermal barrier and a plug potential are produced. The base pressure is less than 5×10^{-8} Torr. A typical plasma density is 3×10^{18} m^{-3} on the axis. An averaged ion temperature is larger than 1.0 keV and an electron temperature is about 100 eV. Because the electron temperature is much lower than the ion temperature, a diamagnetic loop signal is dominated by an ion pressure.

Figure 1 shows an axial profile of the magnetic field strength in the central and the anchor cells. Locations of diagnostics and heating systems are also shown in Fig. 1. Two kinds of ICRF antennas are installed near the mirror throats in the central cell. One kind is the so-called NAGOYA TYPE-III antennas,[19] which are installed at $z=2.2$ m, where the mirror ratio R is 1.6. The other kind is the conventional double half-turn antennas that are installed at the location of $z=\pm1.7$ m, where $R=1.1$. These antennas are driven by two different frequencies of 9.6 and 6.2 MHz. The frequency of 9.6 MHz, corresponding to an ion cyclotron frequency near the midplane of the anchor cell, is required for producing and sustaining plasmas.[20] A compressional Alfvén wave launched from the NAGOYA TYPE-III antenna propagates through a flux tube with an elliptical cross section between the anchor and central cells and is converted into a shear Alfvén wave.[21] The converted shear Alfvén wave is damped in the ion-cyclotron resonance layer in the anchor cell. Therefore, a high-beta plasma is maintained in the anchor cell, which assures MHD stability of the GAMMA 10 tandem mirror plasma. The frequency of 6.2 MHz, corresponding to an ion-cyclotron frequency near the midplane of the central cell, is required for the central-cell ion heating. A plasma is initiated by injecting a short pulse (1 ms) gun-produced plasma from each end and is sustained by applying ICRF power in combination with a hydrogen gas puffing in the central cell. The total radiated power of ICRF antennas is typically 150 kW with a duration of 50 ms. Temperature anisotropy is measured by using a diamagnetic loop array.[22] Three diamagnetic loops are installed at the locations of $z=-0.33$ m, $z=-1.5$ m, and $z=1.95$ m from the central-cell midplane. Mirror ratios at the location of each diamagnetic loop are 1.008, 1.077, and 1.264, respectively. Each diamagnetic loop is named as the midplane loop W_1, the second loop W_2, and the third loop W_3, as shown in Fig. 1. From diamagnetic signals measured by the loop W_2 and another installed at the location of $z=1.5$ m, it is confirmed that an axial pressure profile of the central cell is symmetric with respect to the midplane. Magnetic fluctuations generated in plasmas are mainly measured by using small pickup coils with 2 mm in radius. These magnetic probes measure both r and θ components simultaneously. Signals of the magnetic probe are digitized in eight bits by two channels of a fast Analogue/Digital converter with 100 MHz sampling. By using a conventional fast Fourier transform (FFT) method, signals are converted into the frequency spectra. Cross correlations between two probe signals are analyzed. Magnetic probe arrays both in the axial and azimuthal directions are also used. Probe measurements are mainly limited in peripheral plasma regions in order to avoid disturbances due to the probe insertion. In fact, when the probes are inserted, reductions of both plasma pressures and amplitudes of AIC modes are observed. A radial profile is measured near the mirror throat of the central cell, where a disturbance of the magnetic probe to the core plasma is minor compared to measurements near the midplane. Recently, AIC modes were successfully observed by using a reflectometer system in the GAMMA 10 experiment.[13] Experimentally observed dependences of the AIC amplitude on the beta and temperature anisotropy by use of the reflectometer agree with those obtained from magnetic probe signals.

III. OBSERVATION OF AIC MODES AND THEIR SPATIAL STRUCTURE

A typical time evolution of a line density, diamagnetic signals, and rf input power are shown in Figs. 2(a)–2(c). The rf input power includes a power loss by the circuit. A discharge is initiated by injecting a plasma from a plasma gun. Then, a rf power of 9.6 MHz for producing and sustaining a plasma is launched, as indicated by a dotted line in Fig. 2(c).

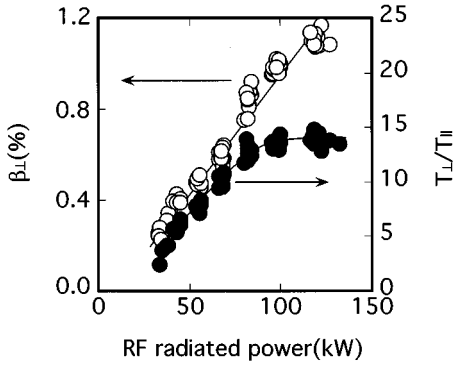

FIG. 3. Radiated power dependence of $\beta_\perp$ and $T_\perp/T_\parallel$ that are evaluated from the signals of a diamagnetic loop array.

When rf power of 6.2 MHz for heating is launched, diamagnetic loop signals begin to increase. The differences among the diamagnetic signals W_1, W_2, and W_3 comes from localization of a plasma pressure, that is, a temperature anisotropy. Hot ions accelerated by the rf field are localized near the midplane where an ion cyclotron resonance layer exists. A line density is measured by the microwave interferometer. After the line density and the diamagnetic signals have reached a steady state, the rf input power is reduced over a 10 ms period. The line density slightly decreases and the diamagnetic loop signals decreases mainly due to the reduction of the ion temperature. By varying the modulation rate of the rf power, a characteristic curve for the ion heating in the central cell is taken. Figure 3 shows a rf power dependence of $\beta_\perp$ and $T_\perp/T_\parallel$, where a product of the density on the axis and the radially averaged temperature are used in evaluating $\beta_\perp$. A parabolic radial profile is also used. The temperature anisotropy $T_\perp/T_\parallel$ is evaluated by using the diamagnetic loop array. The rf radiated power is defined by the rf input power minus the circuit loss power. The value $\beta_\perp$ increases almost linearly with the rf power. Temperature anisotropy also increases with the rf power and reaches about 14 at the rf radiated power of 100 kW and then saturates for a higher rf radiated power. The observed anisotropy should be large enough to induce microscopic instabilities driven by the strong temperature anisotropy and the high plasma beta value. Figure 4 shows a typical frequency spectrum of a θ component of the magnetic fluctuations obtained from the FFT analysis of the probe signal. Peaks at 6.2 and 9.6 MHz in the figure correspond to the frequencies that are externally applied by the rf antennas. The peaks of 5.6–5.9 MHz are spontaneously excited modes. This fluctuation is observed

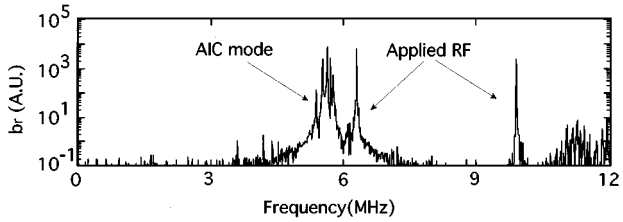

FIG. 4. Typical frequency spectrum of the magnetic probe signal.

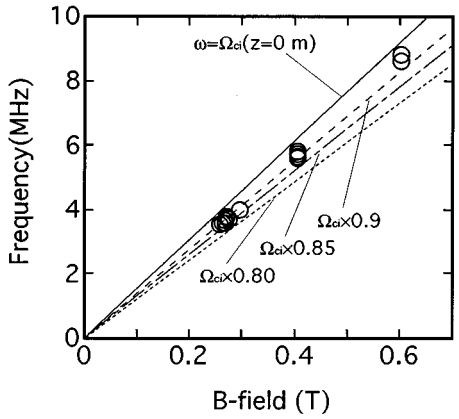

FIG. 5. The magnetic field dependence of the frequency of generated modes.

only when both the anisotropy and the plasma beta value are relatively high. Frequencies of the fluctuations are below the ion cyclotron frequency at the midplane. There are some discrete peaks in the frequency spectrum. Frequency differences between the two adjacent spectral peaks become narrower on the higher-frequency side than those on the lower-frequency side, as shown in Fig. 4. The frequency of the fluctuation depends on the strength of the externally applied magnetic field in the range from 0.3 to 0.6 T, as shown in Fig. 5, where the applied frequency is varied proportional to the magnetic field strength. The measured pressure profiles have a peak in the midplane of the central cell. The solid line indicates the ion cyclotron frequency for the minimum strength of the magnetic field in the central cell. Broken, dotted–broken, and dotted lines correspond to frequencies of $0.9\Omega_{ci}$, $0.85\Omega_{ci}$, and $0.8\Omega_{ci}$, respectively. Here, Ω_{ci} is the ion cyclotron frequency in the midplane. The frequency of the generated mode is slightly below the ion cyclotron frequency in the midplane. This dependence agrees well with studies that predicted a dispersion relation for the AIC mode.

Figure 6 shows a wave structure in the azimuthal direction. The azimuthal mode number m is measured by magnetic probe arrays azimuthally distributed at $z=0.3$ m and measuring the radial component b_r of the fluctuations. Four

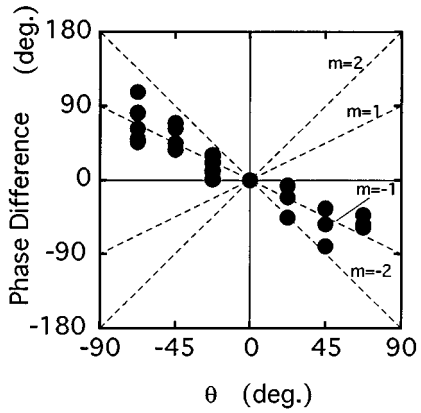

FIG. 6. Phase differences among signals of the magnetic array azimuthally placed.

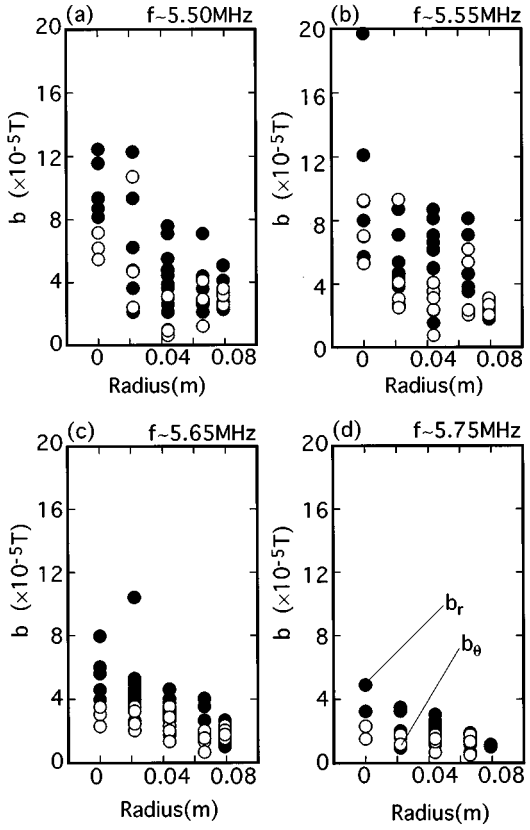

FIG. 7. The radial profile of the amplitude of each discrete peak in the frequency spectrum (a) 5.50 MHz, (b) 5.55 MHz, (c) 5.65 MHz, and (d) 5.75 MHz. Closed and open circles indicate radial and azimuthal components of magnetic fluctuations, respectively.

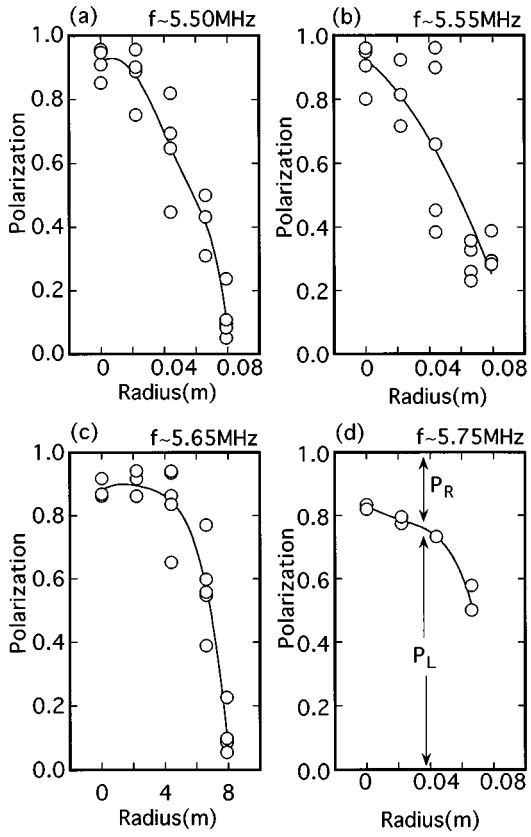

FIG. 8. The radial profile of the polarization for each discrete peak.

magnetic probes are located on the azimuthal angles of 0°, 22.5°, 45°, and 90°. The observed fluctuations have an azimuthal mode number of $m=-1$ or -2. This means that the fluctuations propagate in the ion diamagnetic direction. As indicated in Fig. 4, several peaks are observed in the frequency spectrum. These discrete modes all have a similar azimuthal structure.

Figure 7 shows radial profiles of each mode that are measured at the mirror throat of the central cell. Because ions are accelerated up to a high energy of several keV and are trapped near the midplane of the central cell, most of the high-energy ions cannot reach the mirror throat. Therefore, a disturbance due to insertion of the probe at the throat region is small. The frequencies of each mode are (a) $f\cong 5.50$ MHz, (b) $f\cong 5.55$ MHz, (c) $f\cong 5.65$ MHz, and (d) $f\cong 5.75$ MHz. The amplitude profiles of the radial component b_r as well as the azimuthal component b_θ are plotted in Fig. 7. The fluctuation amplitude are larger in the core region than that in the edge region. This means that the observed modes have the property of body waves and not of surface waves. Polarization profiles that are calculated from the phase difference between b_r and b_θ components are shown in Fig. 8. The polarization in the figure is defined as follows:

$$P_L=\frac{|b_L|^2}{|b_L|^2+|b_R|^2} \quad \text{and} \quad P_R=\frac{|b_R|^2}{|b_L|^2+|b_R|^2}, \tag{3}$$

where

$$b_L=\frac{b_r+ib_\theta}{2} \quad \text{and} \quad b_R=\frac{b_r-ib_\theta}{2}. \tag{4}$$

Here P_L indicates a fraction of a square of a magnetic fluctuation amplitude with a left-handed polarization. Figure 8 shows that the left-handed polarization dominates in the core region of plasmas while the right-handed polarization dominates in the outer region for all discrete modes. This result is consistent with the fact that an AIC mode is a shear Alfvén wave branch caused by free energy for an anisotropic pressure distribution.

The wave structure in the axial direction is evaluated from phase differences between signals of two magnetic probes set along the magnetic field line. An AIC driving term is theoretically given by $\beta_\perp(T_\perp/T_\parallel)^2$. Figure 9 shows an axial wave number $k_\parallel$ as a function of the AIC drive term, where $k_\parallel$ is evaluated from the phase differences. It indicates that phase differences depend on the AIC driving term and converge to zero with the increase in the AIC driving term. The value of the driving term where the phase difference becomes zero is smaller at the position of $z=0.3$ and 0.9 m nearer to the midplane than that at $z=-1.12$ and -1.28 m. The zero phase difference suggests a standing wave structure. The region for the standing wave expands in the z direction with an increase of the AIC driving term. Figure 9 also suggests that the AIC mode has two regions along the magnetic field line: one is a standing wave region near the midplane and the other is a propagating wave outside the standing wave region. This type of Alfvén wave structure

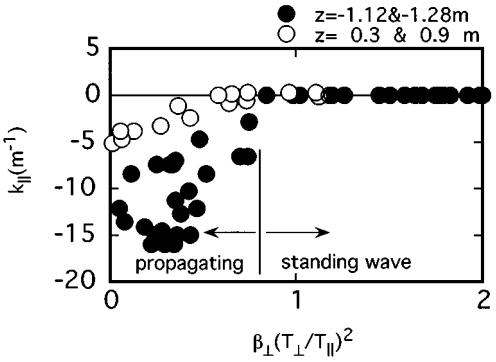

FIG. 9. Axial wave numbers evaluated from phase differences of two magnetic probes located at $z=-1.12$ and -1.28 m and at $z=0.3$ and 0.9 m, which are plotted by solid and open circles, respectively.

has been observed in single mirror experiments with ballooning instabilities.[23] From the measurements of the wave structure in the r, θ, and z direction, each mode is excited as an eigenmode that satisfies the boundary condition in the z direction.

IV. DISCUSSIONS

As predicted in the previous section, observed AIC modes have an axial structure. The dispersion relation of the AIC mode in an infinite and homogeneous plasma is written as follows:[24]

$$D(k,\omega)=k^2c^2-\omega^2+\sum_{j=e,i}\Omega_{pj}^2\chi_j(k,\omega)=0, \tag{5}$$

where Ω_{pj} is the plasma frequency, k is the axial wave number, ω is the frequency of the AIC mode, and χ_j is the plasma susceptibility [see Ref. 24, Eqs. (6)–(11)]. Suffixes i and e denote ions and electrons. Figure 10 shows a typical dispersion relation of the AIC mode that is obtained by solving Eq. (5) with respect to the real wave number k_r, with the temperature anisotropy of 12.5 and $\beta_{\perp}$ of 0.007. The maximum growth rate $[\omega_i/\Omega_{ci}]_{\mathrm{MAX}}$ is defined as a peak value of the imaginary part of the frequency normalized by the cyclotron frequency, which is shown by a dotted–broken line in Fig. 10. The maximum growth rate increases with $\beta_{\perp}$ and temperature anisotropy. In the region of the absolute instability, that is, $\beta_{\perp}(T_{\perp}/T_{\parallel})^2>3.5$, an initial perturbation continuously grows until a nonlinear saturation occurs and the group velocity v_g becomes zero. On the other hand, in the convectively unstable region where $\beta_{\perp}(T_{\perp}/T_{\parallel})^2<3.5$, the amplitude of the instability is determined by the system length. A typical group velocity v_g of the AIC mode with the maximum growth rate $[\omega_i/\Omega_{ci}]_{\mathrm{MAX}}$ is around 3×10^6 m/s. The propagation time of the mode from the generation point to the observation point is about 0.4 μs. Because a growth time of the AIC mode is several tens μs, the amplitude of the fluctuation should not become large enough for detection. In GAMMA 10, however, the AIC mode is observed in the region $\beta_{\perp}(T_{\perp}/T_{\parallel})^2>0.3$. This indicates that an AIC mode can grow to a detectable level in the convectively unstable region for an infinite and a uniform system.

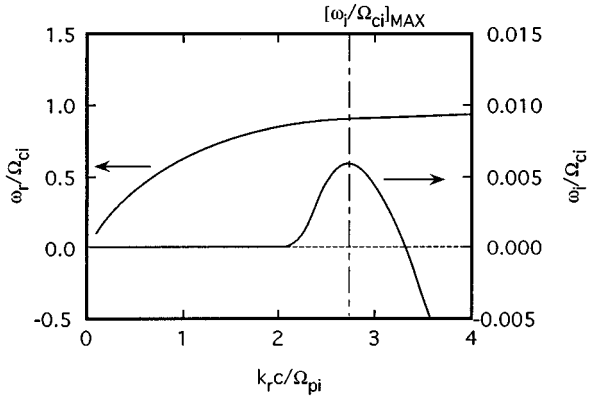

FIG. 10. Dispersion relation of the AIC mode derived from Eq. (5). The maximum growth rate is shown by a dotted-broken line.

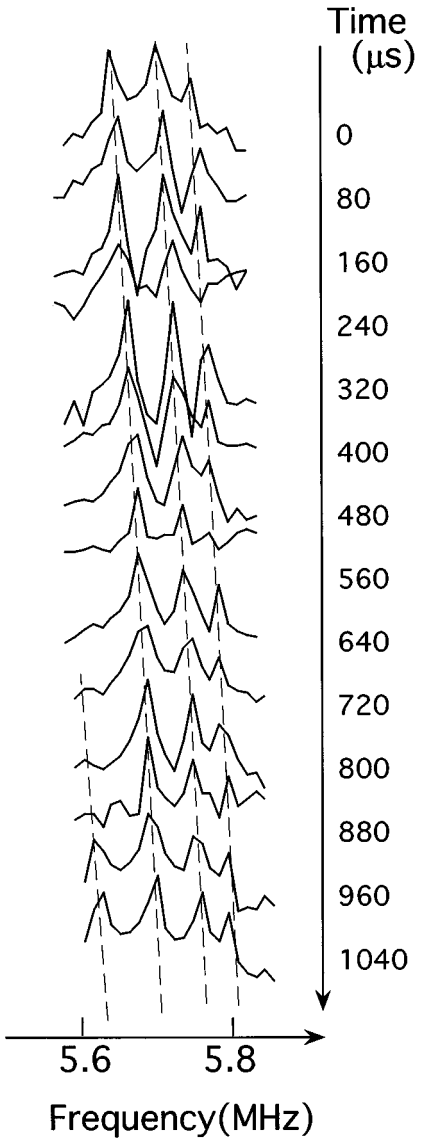

FIG. 11. A time evolution of the frequency spectrum of the AIC mode.

As shown in Fig. 4 and described previously, the frequency spectrum of the AIC mode has discrete peaks. The number of peaks and the frequency of each peak depend on

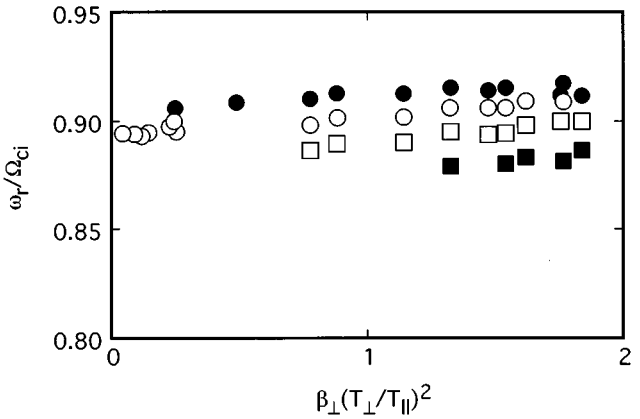

FIG. 12. An AIC driving term's dependence on the frequency of each discrete peak.

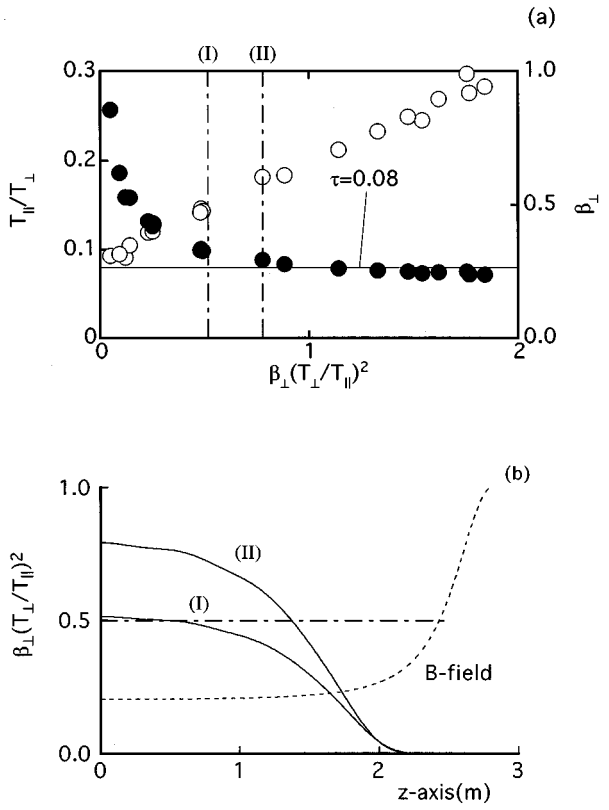

FIG. 13. (a) Dependence of the AIC driving term on beta values and on a reciprocal of temperature anisotropy. For the parameter of (I) and (II), the boundary for the AIC eigenmode occurs near magnetic probes at $z=30$ and 90 cm and at $z=-112$ and -128 cm. (b) An axial profile of the AIC driving term are evaluated for parameters of (I) and (II). The dotted line is the magnetic field strength. The broken-dotted line is the AIC driving term of 0.5, which corresponds to parameters of a reflection point of the AIC mode.

the plasma parameters. In an initial start-up phase, the temperature, density, and temperature anisotropy temporally increase. Temporal variations of the number of peaks and of the frequency of each peak in the start-up phase are clearly seen in Fig. 11. The frequency of the AIC modes shifts toward the higher-frequency side mainly due to an increase in a β value. A new peak appears in the low-frequency side. Figure 12 represents the AIC driving term's dependence on the normalized frequency of the spectral peaks. Plotted points are experimentally obtained. The frequency difference between peaks becomes narrower and the number of the eigenmode increases with the AIC driving term. Figure 13(a) shows the AIC driving term's dependence on the reciprocal of the temperature anisotropy τ and $\beta_\perp$, which are replotted from the data in Fig. 3. As shown in Fig. 13(a), an inverse of the anisotropy is almost constant in the region of $\beta_\perp(T_\perp/T_\parallel)^2>0.8$. Because the temperature anisotropy is almost constant, the increase in the AIC driving term in the region of $\beta_\perp(T_\perp/T_\parallel)^2>0.8$ must be due to the increase in $\beta_\perp$. Figure 13(b) shows the estimated axial profiles of the AIC driving term for different values of the driving term, as indicated by lines (I) and (II) in Fig. 13(a). As described in the previous section, the location of the reflection point varies, depending on the driving term. When the axial profiles of the AIC driving term are (I) and (II), the reflection points happen to be near the magnetic probes, which are installed at $z=0.90$ m and $z=1.28$ m in Fig. 9, respectively. Hence, the boundary length is determined as 1.8 and 2.6 m with respect to (I) and (II) profiles. The critical values of the AIC driving term at the reflection point experimentally obtained are around 0.5 in both cases of lines (I) and (II). The approximated critical value of 0.5 is indicated by the broken-dotted line in Fig. 13(b). The critical value of the AIC driving term of 0.5 is consistent with the stability threshold of the AIC mode that is experimentally obtained in GAMMA 10. When a reflection point appears in the plasma, a standing wave should be formed and excited modes become detectable. Analysis including the inhomogenites in the axial direction is needed for interpretation of the mode excitation. It has been calculated in the previous theoretical work[25] that inhomogeneities in the axial direction work for stabilization of the excited modes rather than for destabilization. In the GAMMA 10 experiments, existence of a reflection point is clearly suggested; however, the mechanism of the reflection and an efficiency of the reflection is still unknown. A new model for the excitation of the AIC mode in a plasma with an axial inhomogeneity is needed.

V. CONCLUSION

Alfvén ion cyclotron (AIC) modes are observed in the ICRF-heated central-cell plasma of the GAMMA 10 tandem mirror. The modes have several discrete frequency peaks in the range slightly below the ion cyclotron frequency in the midplane of the central cell. The frequency spectrum depends on both beta-value and temperature anisotropy. The spatial structures of the mode are measured precisely and are summarized as follows.

(1) The mode propagates in the direction of the ion diamagnetic drift and has the low azimuthal mode number of -1 or -2.
(2) The radial profile of the amplitude is peaked in the core region of the plasma and the left-handed circular polarization is dominant in the core region, while the right-handed circular polarization is dominant near the edge region.

(3) The modes have a standing wave structure in the axial direction in the inner region near the central-cell midplane and a propagating wave structure in the outer region. The extension of the standing wave region depends on the amount of the AIC driving term.
(4) Each discrete peak of the AIC mode has a similar structure in both the azimuthal and radial directions.
(5) The AIC mode is excited as an eigenmode in the axial direction. The location of the boundary is experimentally determined. However, it varies with plasma parameters, and the mechanism of the reflection is still unknown. The threshold for the mode detection can also be explained by the existence of a reflection point.

ACKNOWLEDGMENTS

The authors acknowledge all members of the GAMMA 10 group for carrying out the experiments and for helpful suggestions. They also acknowledge Professor T. Watanabe of the National Institute for Fusion Science for useful discussions about the theoretical model of the AIC mode. The analysis of the diamagnetic flux and the calculation of the dispersion relation for the AIC mode were performed by using the computer system at the Computer Center of the National Institute for Fusion Science.

This work was partly supported by a Grant-in-Aid for Scientific Research from the Ministry of Education and Fellowships of the Japan Society for the Promotion of Science for Japanese Junior Scientists.

[1]J. E. Scharer and A. W. Trivelpiece, Phys. Fluids **10**, 591 (1967).
[2]R. C. Davidson and J. M. Ogden, Phys. Fluids **18**, 1045 (1975).
[3]T. Tajima, K. Mima, and J. M. Dawson, Phys. Rev. Lett. **25**, 201 (1977).
[4]T. D. Rognlien and D. C. Watson, Phys. Fluids **22**, 1958 (1979).
[5]T. Tajima and K. Mima, Phys. Fluids **23**, 577 (1980).
[6]G. R. Smith, Phys. Fluids **27**, 1499 (1984).
[7]M. Tanaka, J. Geophys. Res. **90**, 6459 (1985).
[8]K. T. Tsang and G. R. Smith, Phys. Fluids **30**, 1362 (1987).
[9]A. Iiyoshi, H. Yamamoto, and S. Yoshikawa, Phys. Fluids **10**, 749 (1967).
[10]R. Hatakeyama, M. Inutake, and T. Akitsu, Phys. Rev. Lett. **47**, 183 (1981).
[11]T. A. Casper and G. R. Smith, Phys. Rev. Lett. **48**, 1015 (1982).
[12]M. Ichimura, M. Inutake, R. Katsumata, N. Hino, K. Ishii, T. Cho, M. Hirata, A. Itakura, I. Katanuma, Y. Kiwamoto, A. Mase, S. Miyoshi, Y. Nakashima, T. Saito, T. Tamano, N. Yamaguchi, and K. Yatsu, Plasma Phys. Controlled Nucl. Fusion **34**, 1889 (1992).
[13]A. Mase, M. Ichimura, H. Satake, R. Katsumata, T. Tokuzawa, Y. Ito, H. Hojo, E. J. Doyle, A. Itakura, M. Inutake, and T. Tamano, Phys. Fluids B **5**, 1677 (1993).
[14]T. Tajima and J. M. Dawson, Nucl. Fusion **20**, 1129 (1980).
[15]M. Ichimura, M. Inutake, R. Katsumata, N. Hino, H. Hojo, K. Ishii, T. Tamano, and S. Miyoshi, Phys. Rev. Lett. **70**, 2734 (1993).
[16]G. R. Smith, T. A. Casper and M. J. Gerver, Nucl. Fusion **23**, 1381 (1983).
[17]S. N. Golovato, K. Brau, J. Casey, M. J. Gerver, S. Horne, J. Irby, J. Kesner, B. Lane, J. Machuzak, R. Myer, R. S. Post, E. Sevillano, and L. Wang, Phys. Fluids B **1**, 851 (1989).
[18]M. Inutake, T. Cho, M. Ichimura, K. Ishii, A. Itakura, I. Katanuma, Y. Kiwamoto, Y. Kusama, A. Mase, S. Miyoshi, Y. Nakashima, T. Saito, A. Sakasai, K. Sawada, I. Wakaida, N. Yamaguchi, and K. Yatsu, Phys. Rev. Lett. **55**, 939 (1985).
[19]T. Watari, K. Adati, T. Aoki, S. Hidekuma, K. Hattori, S. Hiroe, M. Ichimura, T. Kawamoto, R. Kumazawa, Y. Okubo, S. Okamura, and T. Sato, Nucl. Fusion **22**, 1359 (1982).
[20]M. Ichimura, M. Inutake, S. Adachi, D. Sato, F. Tsuboi, Y. Nakashima, I. Katanuma, A. Itakura, A. Mase, and S. Miyoshi, Nucl. Fusion **28**, 799 (1988).
[21]M. Inutake, M. Ichimura, H. Hojo, Y. Kimura, R. Katsumata, S. Adachi, Y. Nakashima, A. Itakura, A. Mase, S. Miyoshi, I. Katanuma, Y. Kiwamoto, A. Mase, S. Miyoshi, Y. Nagayama, Y. Nakashima, T. Saito, Y. Tatematsu, N. Yamaguchi, and K. Yatsu, in *Plasma Physics and Controlled Nuclear Fusion Research 1992*, Würzburg (International Atomic Energy Agency, Vienna, 1993), Vol. 2, p. 651.
[22]R. Katsumata, M. Inutake, M. Ichimura, N. Hino, H. Onda, I. Katanuma, H. Hojo, A. Mase, and S. Miyoshi, Jpn. J. Appl. Phys. **31**, 2249 (1992).
[23]R. Hatakeyama, N. Sato, and M. Inutake, Nucl. Fusion **23**, 1467 (1983).
[24]H. Hojo, R. Katsumata, M. Ichimura, and M. Inutake, J. Phys. Soc. Jpn. **62**, 3797 (1993).
[25]G. R. Smith, W. M. Nevins, and W. M. Sharp, Phys. Fluids **27**, 2120 (1984).